Absolute $B(E1)$ values in the shape transitional $^{148-152}$Sm isotopes

A. Jungclaus
Institut Laue-Langevin, F-38042 Grenoble, France
and II. Physikalisches Institut, Universität Göttingen, D-3400 Göttingen, Germany

H. G. Börner, J. Jolie,* and S. Ulbig
Institut Laue-Langevin, F-38042 Grenoble, France

R. F. Casten
Brookhaven National Laboratory, Upton, New York 11973

N. V. Zamfir
Brookhaven National Laboratory, Upton, New York 11973;
Institute of Atomic Physics, Bucharest-Magurele, Romania;
and Clark University, Worcester, Massachusetts 01610

P. von Brentano
Institut für Kernphysik, Universität Köln, D-5000 Köln 41, Germany

K. P. Lieb
II. Physikalisches Institut, Universität Göttingen, D-3400 Göttingen, Germany
(Received 21 September 1992)

The lifetimes of the lowest 3^- and 1^- states in $^{148-152}$Sm have been determined employing the gamma-ray-induced Doppler broadening technique. The $B(E1;3^-\rightarrow 2^+)$ transition rates are compared to the corresponding $B(E1;1^-\rightarrow 0^+)$ values and interpreted in the framework of the interacting boson approximation *sdf* model. The qualitative behavior of these absolute transition rates can be understood in a simple physical picture by considering only the one-body part in the $E1$ transition operator. A more complex form including two-body terms is needed to explain simultaneously all available experimental data related to these levels.

PACS number(s): 21.10.Tg, 21.60.Fw, 23.20.Lv

I. INTRODUCTION

The transition from spherical to quadrupole prolate deformed shapes in the Sm isotopic chain that occurs near $N=88,90$ has attracted much attention from both experimental and theoretical viewpoints. Absolute transition rates, in particular, of $E1$ transitions from the decay of low-lying negative parity states are sensitive quantities which show a dramatic change in nuclear structure across the transitional region [1] and are therefore a decisive test for the reliability of different models. In particular, the interacting boson model (IBM) has been shown to be a versatile model able to explain this transitional region in a simple way [2–4]. Absolute $E1$ transition rates and branching ratios were successfully explained in the framework of the *sdf* IBM by introducing additional two-body terms in the $E1$ operator [2,5].

To date, for $E1$ transitions in this region, the comparison between model predictions and experiment has been restricted to branching ratios and $B(E1;1^-\rightarrow 0^+)$ values, due to the lack of empirical absolute transition rates for the decay of 3^- states. The purpose of this paper is to present the results of a lifetime measurement of the 3^- levels in ^{148,150,152}Sm employing the GRID (gamma-ray-induced Doppler broadening) method [6], which exploits the extraordinary energy resolution of the double-flat-crystal spectrometer GAMS4 [7] at the Institut Laue-Langevin (ILL). This technique takes advantage of the simple fact that the energy of a γ ray emitted from a nucleus which is moving with a certain velocity is shifted relative to a γ ray emitted from a nucleus at rest. In contrast to the traditional Doppler techniques (e.g., DSA and RDDS), the recoil in GRID is not induced by the reaction process but by the electromagnetic decay of the nucleus of interest produced by thermal neutron capture. The recoil velocity and hence the Doppler shift of a subsequently emitted secondary γ ray is therefore smaller by some orders of magnitude and only the unique resolving power of the GAMS4 instrument allows the detection of the small line broadenings. The Doppler profile is essentially determined by three parameters: the lifetime of the state under investigation, the velocity distribution of the excited nuclei at the moment of the γ emission, and the slowing-down process in the target.

Whereas in light nuclei ($A\leq 60$) the feeding pattern,

*Present address: Institut de Physique, Université de Fribourg, Pérolles, CH-1700 Fribourg, Switzerland.

which determines the velocity distribution, is often reasonably well known, this is usually not the case in heavy nuclei due to the more complex deexcitation patterns. In the case of the lowest 1^- state in ^{150}Sm and the 3^- states in ^{148,150}Sm, the experimentally known feeding transitions account only for 32%, 31%, and 64%, respectively, of the total feeding strength of each level. In ^{152}Sm no transition feeding these states is known. This situation, together with the small recoil velocity in heavy nuclei, constitutes a considerable restriction to the precision of GRID lifetime measurements in heavy nuclei.

We have tackled this problem by the following two approaches: (i) We have calculated the original recoil velocity distribution with a statistical model of the nucleus and (ii) in a model-independent way, one can obtain lifetime limits based on extreme feeding scenarios. Previous studies in the heavy nuclei ^{196}Pt [8] and ^{168}Er [9] have shown the power of the GRID method to determine the character of states in these nuclei—even within the limitations of precision mentioned above.

In the present study, we simulated the feeding from a statistical-model description using both a constant-temperature Fermi-gas (CTF) model [10,11] and the Bethe formula [10,11] to calculate the level density and the following parametrizations of the radiative strength functions: the giant dipole resonance model (GDR) for the $E1$ strength, the single particle model for the $E2$, and a global formula, obtained by fitting the experimental radiative dipole strength [12], for $M1$ radiation. Higher multipolarities were not taken into account.

II. EXPERIMENT AND ANALYSIS

For this measurement three targets, consisting each of $\sim$310 mg natural Sm_2O_3 powder contained in carbon holders, were exposed to a thermal neutron flux of 5×10^{14} n/cm^{2}s at the in-pile target position H6-H7 at the ILL high-flux reactor. The isotopic composition of natural Sm allows for the simultaneous investigation of three different isotopes: Whereas ^{148,150}Sm are produced via the (n,γ) reaction, ^{152}Sm is populated via successive neutron capture starting from ^{150}Sm, since ^{151}Sm is unstable but has a large thermal neutron cross section of $\sigma(^{151}\text{Sm})=15.000$ b. Figure 1 shows the line shapes of the 737 and 832 keV γ rays, which depopulate the 3^- and 1^- levels in ^{150}Sm, each obtained in a single scan. All the five measured γ rays were scanned several times and the lifetime values given in Table I were obtained by simultaneous fits of all scans. The errors given are purely statistical. In addition to the values τ_{CTF} and τ_{Bethe}, two more lifetimes are listed which are obtained by using extreme feeding assumptions [13,14]. These lifetimes $\tau_{\max}$ and $\tau_{\min}$ result from the highest and lowest possible recoil velocity. The following assumptions are used for the extreme feeding situations.

(i) $\tau_{\max}$: Each of the experimentally known transitions populating the state I_f^π under investigation is assumed to be the second step of a two-step cascade connecting the capture state I_c^π and I_f^π via an intermediate level I_i^π. The recoil, induced by such a two-step cascade, is the higher the shorter the lifetime of the intermediate state I_i^π. Whereas many of the spins and parities of these states are known, most of their lifetimes are not. Lower lifetime limits of these intermediate levels are then obtained from the recommended upper transition strength limits [15]. The remaining, unknown part of the total feeding strength, not covered by these discrete transitions, is treated as coming directly from the capture state, thus assuring the highest possible recoil.

(ii) $\tau_{\min}$: Again, a feeding via two-step cascades is assumed, but this time with long lifetimes of the intermediate states I_i^π. That means that most of the nuclei are stopped after the first (primary) recoil before the emission of a secondary γ induces again a—this time smaller—recoil. The remaining intensity is in this case added to the feeder transition depopulating the highest of the known intermediate states (implicitly assuming a complete knowledge of the level scheme up to this excitation energy).

These general remarks are complemented by Fig. 2, which illustrates the different feeding scenarios and the corresponding recoil velocity distributions for the 3^- state in ^{150}Sm. This level is fed by 10 experimentally known transitions, which account for 64% of the total decay intensity. The five strongest of them (55%) depopulate states of spin either 2^+ or 4^+, leading to $E1$ multipolarity for the transitions connecting these intermediate states and the 3^- level. For the determination of

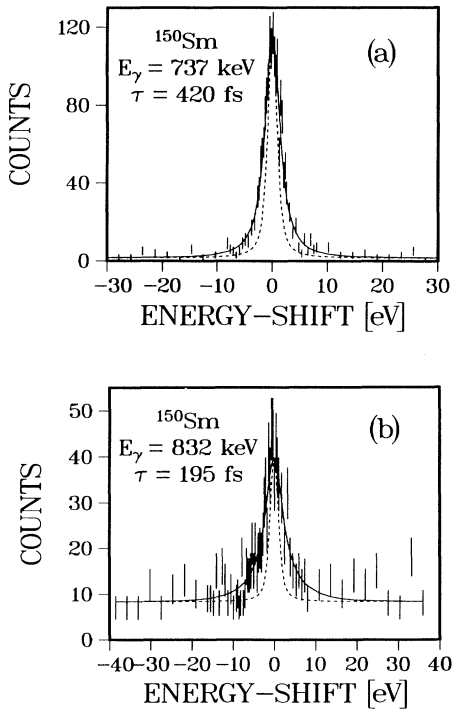

FIG. 1. (a) Doppler broadened line shape of the 737 keV transition which depopulates the 1071 keV level in ^{150}Sm. This lines has been scanned four times and the measuring time was 40 s per point in each scan. The dashed line refers to the instrumental response function. (b) Same as (a) for the 832 keV transition in ^{150}Sm. For this line nine scans have been performed with a measuring time of 200 s per point.

TABLE I. Lifetimes obtained using different approaches to describe the original recoil velocity distributions (see text). The quoted values come from simultaneous fit to all individual scans. The last column gives values from the literature (resonance fluorescence experiments) [16] for comparison.

Nucleus	E_x (keV)	I^π	E_γ (keV)	τ_{CTF} (fs)	τ_{Bethe} (fs)	τ_{min} (fs)	τ_{max} (fs)	$\tau_{Lit.}$ (fs)
^{148}Sm	1161	3^-	611	775^{+530}_{-240}	880^{+605}_{-270}	275^{+370}_{-130}	1270^{+795}_{-365}	
^{150}Sm	1165	1^-	832	195^{+20}_{-15}	185^{+20}_{-15}	60(15)	235(20)	68^{+7}_{-6}
	1071	3^-	737	420(25)	415^{+25}_{-20}	330(20)	650^{+40}_{-35}	
^{152}Sm	963	1^-	842	71^{+18}_{-14}	28^{+12}_{-9}		285^{+50}_{-40}	39(4)
	1041	3^-	919	48^{+11}_{-9}	11^{+7}_{-5}		283^{+35}_{-30}	

τ_{max}, lower lifetime limits of these states were deduced from the upper recommended limit for $E1$ transition rates of $B(E1)=0.01$ W.u. [15] taking into account the correct branching ratios. The resulting values are in the range of 10 fs $<\tau_f<350$ fs. For each of the states which decay via the five remaining known weak transitions (9%) into the 3^- level, a feeder lifetime of 10 fs was assumed. The difference between populating and depopulating γ strength (36%) was accounted for by assuming a primary transition of this intensity (lower part of Fig. 2). τ_{min} was determined under the assumption of long lifetimes ($\tau_f=10$ ps) of the intermediate states and the remaining intensity was attributed to a feeder with energy $E_\gamma=1.1$ MeV assuming that the level scheme is complete up to $\sim$2.2 MeV (upper part of Fig. 2).

If the feeding is effectively from a single feeding transition, then the recoil velocity has only a single discrete value. This case arises either for feeding by a primary transition or through an intermediate level whose lifetime is sufficiently long that previous recoil motion has stopped. On the other hand, if the feeding is through an intermediate level of lifetime comparable to the stopping time, the net recoil velocity is the vector sum of two velocities and is therefore given by a distribution of velocities. Figure 2 shows the recoil velocities from both processes, by discrete thin vertical lines and cross-hatched distributions, respectively. The shift of the average recoil velocity is clearly visible.

The results of the measurement are summarized in Table I and Table II. The values $\tau_{min}=330(20)$ fs and $\tau_{max}=650(^{40}_{35})$ fs for the 3^- level in ^{150}Sm show that, if a part of the feeding pattern is known and the line shape is measured with good statistics, the lifetime can be restricted to a reasonably small range—always bearing in mind

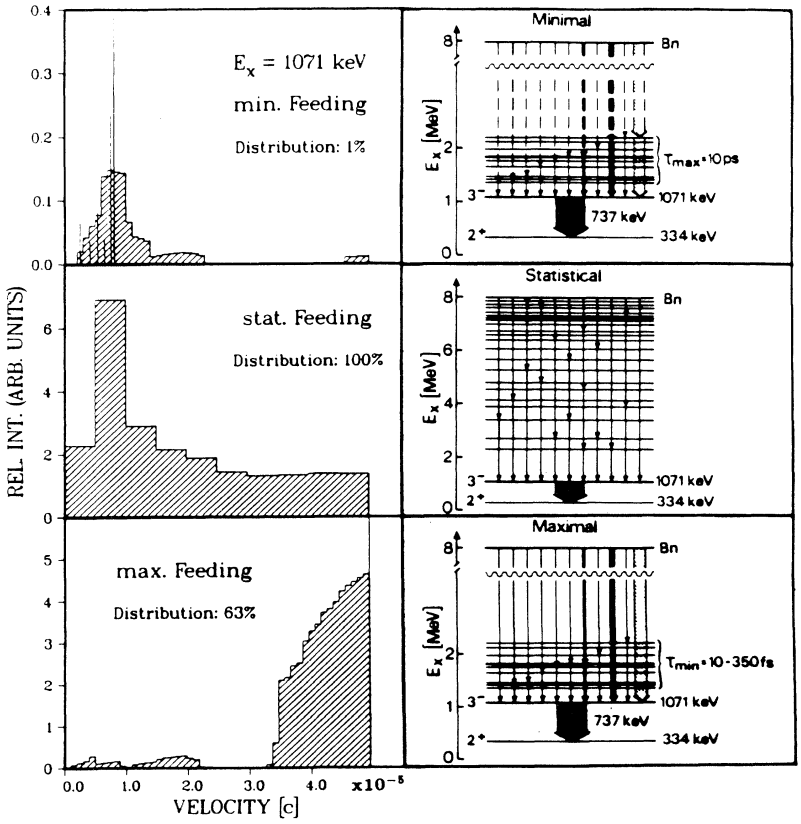

FIG. 2. Illustration of the different feeding scenarios and comparison of the recoil velocity distributions following from these approaches, by means of the 1071 keV (3^-) state in ^{150}Sm. The upper and lower figures represent the two extreme limits compatible with the experimental knowledge of the nucleus. In the middle panel, the deexcitation pattern has been calculated within the statistical approach. In the left part of the figure the two components of the recoil velocity, the discrete and the distributed parts, are shown by discrete thin vertical lines and cross-hatched distributions, respectively. Both are given in arbitrary units. The percentage number shown in each box indicates how many of the recoils arise from the distributed rather than discrete velocity components. See text for further discussion. The shift of the average recoil velocity becomes evident.

TABLE II. Absolute $B(E1)$ transition rates for the decay of the 1^- and 3^- states in ^{148,150,152}Sm. The experimental values (CTF approach) are compared to the calculated transition rates using the operators of Eq. (1) and Eqs. (4)–(7), respectively.

Nucleus	$B(E1;1^-\rightarrow 0^+)$ (10^{-4} e^2fm^2)			$B(E1;3^-\rightarrow 2^+)$ (10^{-4} e^2fm^2)		
	expt.	Eq. (1)	Eqs. (4)–(7)	expt.	Eq. (1)	Eqs. (4)–(7)
^{148}Sm	11(3)[a]	11	18	35^{+24}_{-11}	49	42
^{150}Sm	11(1)	1	8	35(2)	41	29
^{152}Sm	44^{+11}_{-9}	52	64	119^{+27}_{-22}	97	103

[a]From Ref. [16].

the extreme feeding scenarios.

However, some remarks on the listed values (Table I) are appropriate. In ^{148}Sm and ^{150}Sm there is excellent agreement between the lifetimes obtained with the two different level density parametrizations, namely, the CTF model and Bethe formula. The results in ^{152}Sm show that, in the case of short lifetimes, where the fit is most sensitive to the recoil velocity distribution of the decaying nuclei, a strong difference appears with respect to the two statistical models. For the lifetimes of the 1^- states in ^{150}Sm and ^{152}Sm values of $\tau=68^{+7}_{-6}$ fs and $\tau=39(4)$ fs, respectively, were obtained in previous resonance fluorescence experiments [16]. Whereas the value in ^{152}Sm lies between $\tau_{\rm CTF}$ and $\tau_{\rm Bethe}$, the reported lifetime in ^{150}Sm is much smaller than the values obtained from the statistical model approach in the present work. It is consistent with the lower limit deduced from extreme feeding assumptions. $\tau_{\rm Bethe}$ in ^{152}Sm leads to $E1$ transition rates which exceed the recommended upper limit of 0.01 W.u. for the mass region $A=91-150$ [15].

III. DISCUSSION

We restrict the following discussion of the behavior of the absolute transition rates in these three isotopes to the $B(E1)$ values obtained within the CTF approach. These are given in Table II. The qualitative facts to be discussed remain unchanged when using $\tau_{\rm Bethe}$.

Two striking features are immediately obvious. (i) In all three isotopes the $3^-\rightarrow 2^+$ $E1$ transition strengths are noticeably larger than those corresponding to $1^-\rightarrow 0^+$ transitions. The $B(E1;3^-\rightarrow 2^+)$ values remain unchanged from ^{148}Sm to ^{150}Sm and are comparable to that in ^{144}Sm [$50(6)\times 10^{-4}$ e^2fm^2] [17]. (ii) There is an abrupt increase of both the $B(E1;1^-\rightarrow 0^+)$ and the $B(E1;3^-\rightarrow 2^+)$ between $N=88$ and $N=90$. We would like to emphasize that this observation remains valid when using $\tau_{\rm Bethe}$ instead of $\tau_{\rm CTF}$; the increase in $E1$ transition strength is then even more dramatic.

Previous theoretical interpretations of the spherical to deformed transition that take place in the Sm isotopes [2–4] have been associated with the onset and growth of quadrupole collectivity. The IBM provides a convenient formulation in which this evolution of structure can be easily visualized and understood. In the framework of the IBM, the trends of $E1$ strength can also be described in a natural way.

Figure 3 illustrates the structure of the relevant low-lying levels, described within the U(5) limit of the *sdf* IBA model. In this approach an f boson is introduced in addition to the normal *sd*-boson space (the total boson number $N_B=n_s+n_d+n_f$ being conserved) in order to create negative parity excitations. The 3^- level is constructed simply by coupling an $f(l=3)$ boson to the positive parity 0^+ ground state which consists of N_B s bosons and no d bosons. The 1^- state is a member of the two-phonon $[2^+\otimes 3^-]$ quintuplet formed by coupling an f boson to the 2_1^+ state whose boson structure is $|s^{N-1}d\rangle$, that is $n_s=N-1$, $n_d=1$.

If we use the one-body $E1$ operator of the form

$$T^{(E1)}_{sdf}=e_1[d^\dagger\tilde{f}+f^\dagger\tilde{d}]^{(1)}\ , \tag{1}$$

the structure of the U(5) states and this $E1$ operator lead to a qualitative difference in the predicted $B(E1;3^-\rightarrow 2^+)$ and $B(E1;1^-\rightarrow 0^+)$ values that can be tested by the present measurements. The $1^-\rightarrow 0^+$ transition must involve the destruction of *both* an f boson *and* a d boson (and the concommitent creation, therefore, of two s bosons). This is impossible with the structure of the $E1$ operator in Eq. (1) which can create or destroy only a single f boson (and destroy or create a d boson). Thus the $1^-\rightarrow 0^+$ $E1$ transition is *forbidden* in the strict U(5) limit with the operator of Eq. (1).

In contrast, the $3^-\rightarrow 2^+$ transition is *allowed*. It involves the destruction of an f boson and creation of a d boson which can be achieved with the first term of Eq. (1). Hence, the U(5) limit immediately gives a simple prediction

$$\frac{B(E1:1^-\rightarrow 0^+)}{B(E1;3^-\rightarrow 2^+)}\ll 1\ . \tag{2}$$

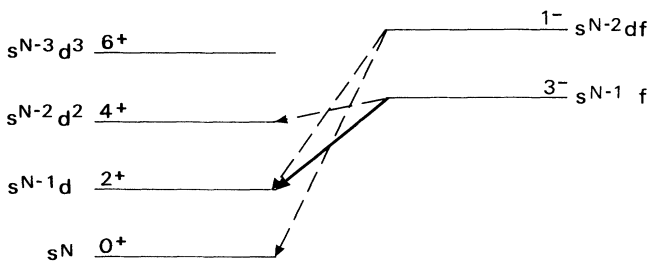

FIG. 3. Boson structure of the yrast states in the vibrational U(5) limit of the *sdf* IBM. The solid line corresponds to an allowed $E1$ transition and the dashed lines mark transitions which are forbidden for the one-body operator of Eq. (1).

A second qualitative feature emerges when U(5) is broken, for example, in the shape transition [U(5)→SU(3)] that occurs in the Sm isotopes between $N=86$ and 90. Any interaction that induces such a structural change, e.g., the $Q\cdot Q$ interaction in the IBM, will mix the U(5) basis states. The main features can be understood with the simple IBM-1 Hamiltonian

$$H=\epsilon n_d-\kappa Q\cdot Q \tag{3}$$

where Q is the usual *sd*-boson quadrupole operator.

The spherical-deformed phase transition is induced both by changes in boson number (since the matrix elements of the $Q\cdot Q$ term increase faster than those of the n_d term with the boson number N_B) and by changes in κ/ϵ. Nevertheless, the effects on the wave functions can be seen in a schematic calculation with constant N_B. We choose a very low boson number, $N_B=4$, for this purpose so that the mixing of U(5) basis states is easier to see. Table III gives the wave functions of $N_B=4$ for four κ/ϵ values, which increase in the U(5)→SU(3) transition region. We note that the empirical energy ratio $R=E_{4_1^+}/E_{2_1^+}$ has specific values for the dynamical symmetries and increases smoothly from 2.00 in the U(5) limit to 3.33 in SU(3); there is a one-to-one relation between κ/ϵ and the *empirical* ratio $E_{4_1^+}/E_{2_1^+}$. The sequential increase in mixing is evident in the table for the larger R and κ/ϵ values (and would be exacerbated if N_B were to be increased as occurs in realistic calculations). This mixing in the 1^- and 0^+ states leads to several finite contributions to the $E1$ matrix element. Hence, except in the unlikely case of complete cancellation, it must give an increasing $1^-\rightarrow 0^+$ transition strength. The last column of Table III shows the calculated $B(E1;1^-\rightarrow 0^+)$ values (arbitrary units) for the wave functions in the table assuming the $E1$ operator of Eq. (1). The increase is evident. Such effects, of course, would be increased when larger, and increasing, N_B values are considered (see below Fig. 4—right). The effects of mixing on the *already* allowed $3^-\rightarrow 2^+$ transition are less obvious from such a schematic calculation, but it is certainly plausible that any increase will be less dramatic.

These conclusions are verified in calculations with larger boson numbers. This is illustrated in Fig. 4 (left), which shows calculated matrix elements for several transitions obtained for a sequence of κ/ϵ values (E_{4^+}/E_{2^+} values) and $N_B=9$. The increase in boson number, which usually accompanies the spherical-deformed transition,

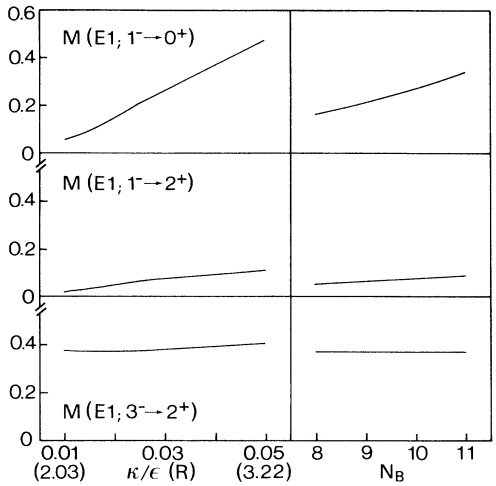

FIG. 4. Calculated matrix elements for the $1^-\rightarrow 0^+$, $1^-\rightarrow 2^+$, and $3^-\rightarrow 2^+$ transitions. Left side: Variable ϵ (the corresponding ratio $R=E_{4^+}/E_{2^+}$ is given in parentheses) and constant $N_B=9$, $\kappa=0.05$, and $\chi=-2.958$. Right side: Variable boson number N_B and constant $\epsilon=2.0$, $\kappa=0.05$, and $\chi=-0.5$ ($\kappa/\epsilon=0.025$).

enhances the trend to increase the $1^-\rightarrow 0^+$ and, although less dramatic, the $3^-\rightarrow 2^+$ matrix elements (Fig. 4—right). From both these contributions we arrive at two qualitative results: First, the $B(E1;1^-\rightarrow 0^+)/B(E1;3^-\rightarrow 2^+)$ transition ratio should be small in the vibrational Sm isotopes and, secondly, this ratio should increase across the spherical-deformed transition region in the Sm isotopes. This discussion points to the importance of the new measurements of the absolute $E1$ $3^-\rightarrow 2^+$ transition rates, especially in the more vibrational Sm isotopes, where these $B(E1)$ values highlight the contrast between the allowed nature of the $3^-\rightarrow 2^+$ transition and the forbidden $1^-\rightarrow 0^+$ case which is an inherent feature of the vibrational limit. This is significant since previous detailed calculations [2,5] of the $1^-\rightarrow 0^+$ transitions, though successful, were quite complex and did not reveal so clearly the origin of these transitions.

Although these schematic calculations reproduce the experimental trends of the $1^-\rightarrow 0^+$ and $3^-\rightarrow 2^+$ transition rates, it has been pointed out by Scholten *et al.* [2] that in the *sdf* space a simple one-body $E1$ operator is unable to describe all the observed $E1$ transition rates. In fact this can be easily seen in Fig. 4: The

TABLE III. Wave functions of the 0_1^+ and 1_1^- states for boson number $N_B=4$, expressed in the U(5) basis ($n_d\, n_\beta\, n_\Delta\, L_d$). Only the transitions (1002)→(2100), (2002)→(3010), and (3102)→(4200) are allowed. The last column gives the transition rates in arbitrary units.

		0_1^+				1_1^-			
κ/ϵ	$R=E_{4_1^+}/E_{2_1^+}$	(0000)	(2100)	(3010)	(4200)	(1002)	(2002)	(3102)	$B(E1;1_1^-\rightarrow 0_1^+)$ (arb. units)
0.0	2.0	1	0	0	0	1	0	0	0
0.05	2.21	0.967	0.252	−0.008	0.019	0.994	−0.039	0.101	9
0.15	2.43	0.855	0.511	−0.037	0.079	0.976	−0.085	0.199	37
0.5	2.55	0.726	0.667	−0.075	0.151	0.947	−0.135	0.292	67

relatively small $1^- \rightarrow 2^+$ transition strength cannot reproduce the experimentally large $B(E1;1^- \rightarrow 2^+)/B(E1;1^- \rightarrow 0^+) \sim 2.0$ branching ratio in all transitional Sm isotopes. The same problem arises for the $B(E1;3^- \rightarrow 4^+)/B(E1;3^- \rightarrow 2^+)$ branching ratio: All the schematic calculations shown in Fig. 4 predict $M(E1;3^- \rightarrow 4^+)=0$ and the experimental value is ~ 1 for ^{150,152}Sm. For a reasonable description it seems to be necessary either to include higher-order terms [2] or to consider the full *spdf* space [20–22]. In the former case, one has to deal with the problem of choosing only a few appropriate two-body terms out of the many possible in order to keep the number of parameters as low as possible, whereas in the latter case, there are already as many as three free parameters in the one-body $E1$ transition operator.

To address this issue we exploit the results of a recent study that combines these two approaches by proposing an effective *sdf* IBA $E1$ operator [5], which contains both one-body and two-body terms. This operator was obtained by coupling an additional p degree ($l=1$) of freedom to the *sdf* bosons without really considering the full *spdf* space: Under the assumption that small admixtures of p bosons are already sufficient to explain the experimentally observed behavior of $E1$ transitions [20], the p boson can be eliminated from the *spdf* space by perturbation theory. The new effective *sdf* $E1$ operator includes two additional two-body terms relative to Eq. (1) and is given by

$$T^{(E1)}_{sdf} = e_1[(d^\dagger \tilde{f} + f^\dagger \tilde{d})^{(1)} + \chi_1 O_1 + \chi_1' O_1'] \quad (4)$$

where O_1 and O_1' are the following two-body terms:

$$O_1 = [Q^{(2)}_{sd} \times (s^\dagger \tilde{f} + f^\dagger s)^{(3)}]^{(1)} , \quad (5)$$

$$O_1' = \sum \sqrt{2l+1}(-1)^{l+1} \begin{Bmatrix} 2 & 1 & 1 \\ 2 & 3 & l \end{Bmatrix} A \quad (6)$$

$$A = [Q^{(2)}_{sd} \times (d^\dagger \tilde{f} + f^\dagger \tilde{d})^{(l)}]^{(1)}$$

and where

$$Q_{sd} = (s^\dagger \tilde{d} + d^\dagger s)^{(2)} + \chi_2 (d^\dagger \tilde{d})^{(2)} \quad (7)$$

is the usual *sd*-boson quadrupole operator. This operator has been tested in some deformed rare-earth nuclei [5,18] and also recently applied to higher spin states in the Sm isotopes [19].

We have therefore used this approach, trying to keep the number of parameters to a minimum. Figure 5(a) illustrates these calculations, showing predictions for both $E1$ transitions calculated with the Hamiltonian of Scholten *et al.* [2] and the $E1$ operator of Eqs. (4)–(7). The effective $E1$ charge was kept constant ($e_1=0.22$ e fm) in order to see if the internal structure of the $E1$ operator [Eqs. (4)–(7)] is able to reproduce the sharp increase of the transition strength. For the other parameters the values $\chi_1=-0.014$ and $\chi_1'=0.38$, 0.12, and -0.08 for ^{148}Sm, ^{150}Sm, and ^{152}Sm, respectively, were used. The calculations reproduce the large ratio $B(E1;3^- \rightarrow 2^+)/B(E1;1^- \rightarrow 0^+) \sim 3$ that is seen experimentally. They also correctly give the sharp increase in both $B(E1;3^- \rightarrow 2^+)$ and $B(E1;1^- \rightarrow 0^+)$ values between ^{150}Sm and ^{152}Sm that reflects the changing structure of the wave functions that accompany the rapid shape change at the neutron number $N=90$. This $E1$ operator is also able to describe the $B(E1)$ branching ratios for the decay of the 1^- and 3^- states whereas the simple operator of Eq. (1) fails, as is shown in Fig. 5(b).

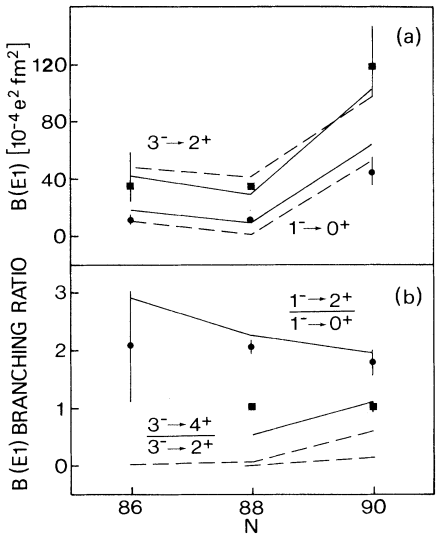

FIG. 5. (a) Transition rates for the decay of the 1^- and 3^- states in ^{148,150,152}Sm. The experimental values (τ_{CTF}) are marked by symbols. The dashed lines show the calculations using the one-body operator of Eq. (1) and the solid lines present the values obtained with the full $E1$ operator of Eqs. (4)–(7). (b) $B(E1)$ branching ratios for the decay of the 1^- and 3^- states in ^{148,150,152}Sm. The convention for solid and dashed lines is the same as in (a).

IV. CONCLUSION

We presented the results of a GRID lifetime measurement in the even-even $^{148-152}$Sm isotopes. The main uncertainty involved in the application of the GRID technique to heavy nuclei is the incomplete knowledge of the γ flux populating the state under investigation. This problem has been discussed in detail and different possibilities to tackle it (simulation of the decay pattern within a statistical model, assumption of extreme feeding scenarios) have been studied. Lifetime values for the lowest 1^- and 3^- states in these isotopes were presented and interpreted in terms of the *sdf* IBM. Considering a simple one-body $E1$ operator and the structure of the U(5) basis states, the qualitative behavior of the $E1$ transition strengths could be related to the changing structure of the wave functions involved when deformation sets in. More detailed calculations with higher-order terms in the $E1$ operator gave better agreement, especially for the spin-increasing transitions.

ACKNOWLEDGMENTS

We would like to thank Dr. E. Kessler and Dr. R. W. Deslattes for their contributions in maintaining and improving the GAMS4 spectrometer. This work has been supported in part by the U.S. Department of Energy under Contract Nos. DE-AC02-76CH00016 and DE-FG02-88ER40417.

[1] A. Bohr and B. R. Mottelson, *Nuclear Structure* (Benjamin, New York, 1975), Vol. II.
[2] O. Scholten, F. Iachello, and A. Arima, Ann. Phys. (N.Y.) **115**, 325 (1978).
[3] O. Castaños, A. Frank, and P. Federman, Phys. Lett. **88B**, 203 (1979); O. Castaños, P. Federman, A. Frank, and S. Pittel, Nucl. Phys. **A379**, 61 (1982).
[4] M. M. King Yen, S. T. Hsieh, H. C. Chiang, and D. S. Chuu, Phys. Rev. C **29**, 688 (1984).
[5] N. V. Zamfir, O. Scholten, and P. von Brentano, Z. Phys. A **337**, 293 (1990).
[6] H. G. Börner, J. Jolie, F. Hoyler, S. Robinson, M. S. Dewey, G. Greene, E. Kessler, and R. D. Deslattes, Phys. Lett. B **215**, 45 (1988).
[7] M. S. Dewey, E. G. Kessler, G. L. Greene, R. D. Deslattes, H. G. Börner, and J. Jolie, Nucl. Instrum. Methods Phys. Res. **A284**, 151 (1989).
[8] H. G. Börner, J. Jolie, S. Robinson, R. F. Casten, and J. A. Cizewski, Phys. Rev. C **42**, R2271 (1990).
[9] H. G. Börner, J. Jolie, S. J. Robinson, B. Krusche, R. Piepenbring, R. F. Casten, A. Aprahamian, and J. P. Draayer, Phys. Rev. Lett. **60**, 691 (1991).
[10] T. v. Egidy, H. H. Schmidt, and A. N. Behkami, Nucl. Phys. **A481**, 189 (1988).
[11] B. Krusche and K. P. Lieb, Phys. Rev. C **34**, 2103 (1986).
[12] J. Kopecky, Inst. Phys. Conf. Ser. No. 62, 423 (1981).
[13] H. G. Börner, J. Jolie, S. J. Robinson, E. G. Kessler, S. Ulbig, R. F. Casten, S. M. Dewey, G. Greene, R. Deslattes, K. P. Lieb, B. Krusche, and J. A. Cizewski, in *Capture Gamma-Ray Spectroscopy,* Proceedings of the Seventh International Symposium on Capture Gamma-Ray Spectroscopy and Related Topics, edited by R. W. Hoff, AIP Conf. Proc. No. 238 (AIP, New York, 1991), p. 173.
[14] S. Ulbig, J. Jolie, H. G. Börner, M. S. Dewey, K. P. Lieb, and S. J. Robinson, in *Capture Gamma-Ray Spectroscopy* [13], p. 396.
[15] P. M. Endt, At. Data Nucl. Data Tables **26**, 47 (1981).
[16] F. R. Metzger, Phys. Rev. **137**, B1415 (1965); Phys. Rev. C **14**, 543 (1976).
[17] A. F. Barfield, P. von Brentano, A. Dewald, K. O. Zell, N. V. Zamfir, D. Bucurescu, M. Ivaşcu, and O. Scholten, Z. Phys. A **332**, 29 (1989).
[18] P. von Brentano, N. V. Zamfir, and A. Zilges, Phys. Lett. B **278**, 221 (1992).
[19] N. V. Zamfir and P. von Brentano, Phys. Lett. B **289**, 245 (1992).
[20] J. Engel and F. Iachello, Nucl. Phys. **A472**, 61 (1987).
[21] D. F. Kuznezov and F. Iachello, Phys. Lett. B **209**, 420 (1988).
[22] T. Otsuka and M. Sugita, Phys. Lett. B **209**, 140 (1988).